Icarus **156**, 296–301 (2002)
doi:10.1006/icar.2001.6787, available online at http://www.idealibrary.com on IDEAL®

NOTE

Detection of the Forbidden SO $a^1\Delta \rightarrow X^3\Sigma^-$ Rovibronic Transition on Io at 1.7 μm

Imke de Pater

Department of Astronomy and Department of Earth and Planetary Sciences, University of California, Berkeley, California 94720
E-mail: imke@floris.berkeley.edu

Henry Roe and James R. Graham

Department of Astronomy, University of California, Berkeley, California 94720

Darrell F. Strobel

Department of Earth and Planetary Sciences and Department of Physics and Astronomy, Johns Hopkins University, Baltimore, Maryland 21218

and

Peter Bernath

Department of Chemistry, University of Waterloo, Waterloo, Ontario, Canada N2L 3G1

Received August 17, 2001; revised October 31, 2001

We report the discovery of the forbidden electronic $a^1\Delta \rightarrow X^3\Sigma^-$ transition of the SO radical on Io at 1.7 μm with the W. M. Keck II telescope on 24 September 1999 (UT), while the satellite was eclipsed by Jupiter. The shape of the SO emission band suggests a rotational temperature of $\sim$1000 K; i.e., the gas is extremely hot. We interpret the observed emission rate of $\sim 2 \times 10^{27}$ photons s^{-1} to be caused by SO molecules in the excited $a^1\Delta$ state being directly ejected from the vent at a thermodynamic quenching temperature of $\sim$1500 K, assuming a SO/SO$_2$ abundance ratio of $\sim$0.1 and a total venting rate of $\sim 10^{31}$ molecules s^{-1} (Strobel and Wolven 2001, *Astrophys. Space Sci.* 277, 1–17). The shape of our complete (1.6–2.5 μm) spectrum suggests that the volcano Loki contains a small ($\sim$2 km^2) hot spot at 960 ± 12 K, as well as a larger ($\sim$50 km^2) area at 640 ± 5 K.

Key Words: **Io; infrared observations; volcanism; atmosphere composition; atmosphere structure.**

Introduction. Io, with its tidal-heating-driven volcanoes and complex interaction with Jupiter's magnetosphere, is one of the most remarkable bodies in our Solar System. Although the satellite has been studied extensively by spacecraft, many questions regarding the nature of its volcanic eruptions remain unanswered. For example, why are hot-spot temperatures associated with volcanoes having long-lived plumes (e.g., Prometheus) usually at $\lesssim$650 K, while intermittent short-lived volcanoes sometimes display temperatures of over 1500 K (e.g., Pele; Lopes *et al*. 2001)? How often do volcanoes erupt, and which events lead to plume activity? It appears as if only a fraction of the hot spots are associated with volcanic plumes.

Pearl *et al*. (1979) identified gaseous sulfur dioxide near Loki Patera in Voyager IRIS (infrared spectrometer) spectra, a gas which was later detected more globally with the 30-m IRAM (Institut de Radio-Astronomie Millimétrique) telescope at millimeter wavelengths (Lellouch *et al*. 1990, 1992) and with HST (Hubble Space Telescope) at UV wavelengths (Ballester *et al*. 1994). These observations suggest that the atmosphere consists of SO_2 gas in equilibrium with SO_2 frost on the surface, in addition to, and probably dominated by, a volcanic source of sulfur dioxide gas (Lellouch 1996). The presence of spatial variations in the SO_2 column density across Io's disk was finally conclusively shown by McGrath *et al*. (2000). They used spatially resolved spectroscopic observations from the HST to show that the SO_2 column density was $\sim$5 times higher above Pele than above a nonvolcanic region. These authors further detected S and inferred SO at abundances S/SO/SO$_2$ = 0.3–0.7/3–20/100, where the relative inferred SO abundance is consistent with disk-averaged measurements by Lellouch *et al*. (1996). The shape of Lellouch *et al*.'s (1990, 1992) SO_2 millimeter line suggests a high atmospheric temperature at a few nanobars pressure, which Strobel *et al*. (1994) could only match with a thermal model of Io's atmosphere at significantly lower, subnanobar pressures, but not at a few nanobars. Strobel *et al*. concluded that Joule heating could raise the temperature at very low pressures near the exobase to as much as 2000 K.

When Io is in eclipse, the satellite itself is invisible but "glows" through its hot spots. We choose such a time to observe the satellite at mid- and near-infrared wavelengths with both Keck telescopes to determine Loki's hot-spot temperature and to search for emission features. In this Note we report the near-infrared spectra; the full dataset will be presented in a future paper.

Observations. We observed Io with the near-infrared spectrometer NIRSPEC on the 10-m W. M. Keck II telescope on 24 September 1999 (UT). We observed Io in sunlight before the satellite went into eclipse and continued observing until Io disappeared behind Jupiter. NIRSPEC is equipped with a 1024×1024 InSb ALADDIN array for spectroscopy. We used four different settings (see Table I) in the 1–2.5 μm range in low-resolution ($R \sim 2000$) mode,

0019-1035/02 $35.00

TABLE I
Log of the Observations, 24 September 1999 (UT)[a]

Time (hr:min)	Object	Int. time (s)	Frames	Separation[b] (″)	Airmass	Setting name	λ_1–λ_2 (μm)	Comments
9:11	SJ9182	2 × 30	207–208		1.35	N-6b	1.92–2.35	
9:19	SJ9182	3 × 30	209–211		1.38	N-6a	1.57–2.00	
9:56	SJ9182	3 × 30	225–227		1.60	N-6a	1.57–2.00	
10:30	Io	4 × 10[c]	244–247	46.0	1.25	N-7	2.23–2.66	Sunlit
10:34	Io	2 × 10[c]	248–249	44.6	1.12	N-6b	1.92–2.35	Sunlit
10:37	Io	2 × 10[c]	250–251	43.7	1.10	N-6a	1.57–2.00	Sunlit
10:39	Io	2 × 10[c]	252–253	43.0	1.10	N-4	1.32–1.61	Sunlit
10:48	Io	2 × 10[c]	254–255	40.0	1.09	N-4	1.32–1.61	Sunlit
10:59	Io	2 × 20	263–264	36.4	1.07	N-6b	1.92–2.35	Eclipse
11:02	Io	2 × 30	265–266	35.4	1.06	N-6a	1.57–2.00	Eclipse
11:05	Io	2 × 30	267–268	34.4	1.06	N-6a	1.57–2.00	Eclipse
11:09	Io	2 × 30	269–270	33.1	1.05	N-6b	1.92–2.35	Eclipse
11:12	Io	2 × 30	271–272	32.1	1.05	N-6a	1.57–2.00	Eclipse
11:15	Io	2 × 30	273–274	31.1	1.05	N-7	2.23–2.66	Eclipse
11:18	Io	2 × 30	275–276	30.1	1.04	N-6b	1.92–2.35	Eclipse
11:22	Io	2 × 30	277–278	28.8	1.04	N-6a	1.57–2.00	Eclipse
11:33	Io	6 × 30	279–284	25.2	1.04	N-7	2.23–2.66	Eclipse
13:13	SJ9105	3 × 30	298–300		1.04	N-7	2.23–2.66	
13:18	SJ9105	2 × 30	305–306		1.04	N-6b	1.92–2.35	
13:30	SJ9105	2 × 25	317–318		1.05	N-4	1.32–1.61	

[a] At the time of the observations, Io was at a heliocentric distance $r = 4.955$ AU and geocentric distance $\Delta = 4.083$ AU.
[b] Io's approximate offset from Jupiter's center. One jovian radius is 24.15″.
[c] Total integration per scan is 10 s; these consists of 40 co-adds of 0.25 s each.

with a slit width of 0.76″, length of 42″, and pixel size of 0.144″ (McLean *et al*. 2000). There is also a slit-viewing camera (SCAM), which consists of a 256 × 256 HgCdTe PICNIC array of 0.18″ pixels, yielding a field of view 46″ square. Figure 1a shows an image of the SCAM field of view: Jupiter is clearly seen, with the slit to the right (west), on the eclipsed satellite Io. On the inset (panel b) we show a blowup of Io in eclipse when off the slit. The bright volcano Loki is visible on the right side, and the fainter Kanehikili–Janus complex is to the left.

Spectra in different settings were taken before Io went into eclipse, and while the satellite was eclipsed by Jupiter (Table I). The various settings overlapped slightly in wavelength to aid reconstruction of a composite spectrum. The spectral settings were calibrated using standard argon and neon lamps and fine tuned with help of telluric OH lines. The final wavelength calibration is accurate to ∼1 Å. Spectra of the stars SJ9182 and SJ9105 (Persson *et al*. 1998), both G4 stars, were taken several times during the night to correct for atmospheric absorption. All data were flatfielded, and bad pixels were removed. The spectra of Io and calibration stars were usually taken with the object at different positions on the slit; subtraction of adjacent spectra successfully removed most of the sky background (i.e., atmospheric lines) and created a positive and negative spectrum of the object on the final "image" (Fig. 1c). All spectra were rectified so that wavelength runs along the y coordinate and the spatial direction runs along x. To create high signal-to-noise one-dimensional spectra we averaged columns over the object (10 pixels on Io, 5 pixels on the star) and subtracted the residual sky background from each spectrum by averaging the sky to the left and right of the positive and negative spectral traces of the object (Fig. 1c). This procedure results in clean Io spectra, albeit not yet corrected for terrestrial absorption.

To correct for the Earth's atmospheric absorption, we divided the individual Io spectra by an average spectrum of the observed G4 stars. Since the spectrum of these stars resembles a solar spectrum, our Io spectra at this point are "normalized" to that of the Sun. A composite spectrum of "Io-in-sunlight" is shown in Fig. 2a. This spectrum is indeed relatively flat, as would be expected for a gray body visible in reflected sunlight. The overall spectral shape is quite similar to Galileo NIMS data of SO_2-frost covered areas on Io (Douté *et al*. 2001), but the reddening longwards of ∼2.2 μm is probably influenced by thermal emission from Io's hot spots (Loki was particularly active in late September–December 1999; Howell *et al*. 2001). The data gaps at wavelengths $1.35 < \lambda < 1.45$ μm and $1.80 < \lambda < 1.95$ μm are at regions of high opacity in the Earth's atmosphere. The apparent emission feature near 2 μm is caused by CO_2 in the Earth's atmosphere; it is seen in absorption in the Io and star spectra and was overcorrected via division by the stellar spectrum.

To remove the effect of the G4 stars, we multiplied the "Io-in-eclipse" spectra by a normalized solar spectrum (Colina *et al*. 1996) to obtain the intrinsic spectral shape of Io's thermal emission. Figure 2b shows Io's spectrum while the satellite was in eclipse, averaged over the duration of the eclipse, in photons s^{-1} cm^{-2} μm^{-1} (the calibration is explained in the next section). In addition to the Earth's atmospheric CO_2, a second emission band shows up in the 'Io-in-eclipse' data near 1.7 μm. This is the band we identified with the forbidden electronic transition of the SO radical. Figures 2c and 2d show blowups of this SO band after subtraction of the blackbody background spectrum (the black line). The rise in intensity at $\lambda \lesssim 1.6$ μm is caused by scattered light from Jupiter. Jupiter is very bright in reflected sunlight, except in methane and collision-induced hydrogen absorption bands. The planet is therefore relatively dark in the wavelength region $1.63 < \lambda < 2.5$ μm.

Although we show one final (averaged) spectrum in Fig. 2, we obtained several spectra in each setting over the duration of the eclipse (Table I). The measured intensity of the spectra varied substantially from scan to scan (by up to factors of ∼3; the scan overplotted on Fig. 1 shows one of the largest measured intensity variations); this is likely caused by imperfect pointing of the telescope. The slope of individual spectra in each setting, however, was stable to within 2%. We note that the stability of the continuum slope also shows that we have minimal residual error in the slope due to scattered light from Jupiter. If Jupiter were influencing the slope of Io's spectrum, its signal would increase while Io is approaching Jupiter, analogous to the strong increase in intensity we measured at $\lambda \lesssim 1.6$ μm over the course of the observations.

Calibration scale and hot-spot temperature(s). We can use the spectral shape in Fig. 2b to derive the temperature of the hot spots on Io which contribute to the observed intensity. The best-fit blackbody curve for a single temperature

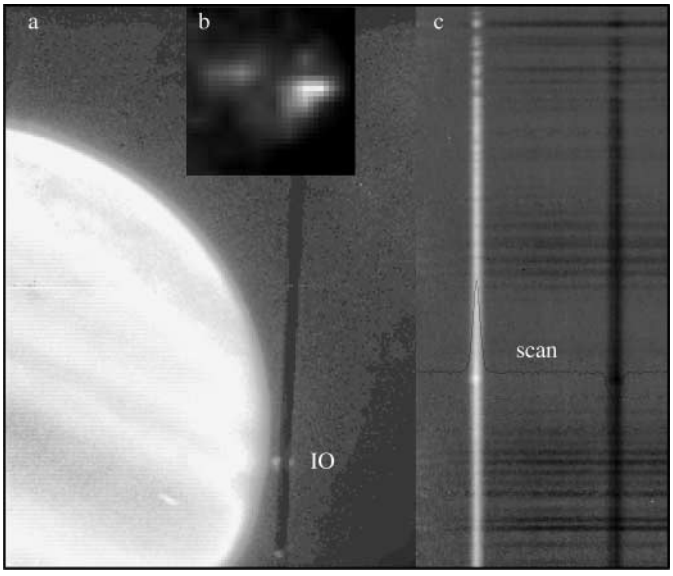

FIG. 1. Overview of the observing conditions. The large panel (a) shows the SCAM field of view, with Jupiter on the left and Io in Jupiter's shadow (indicated by IO), covered by the NIRSPEC slit. This image was taken with the NIRSPEC-7 blocking filter toward the end of our observations (11:26 UT). The scale along the y axis is $46''$. Panel (b) shows a blowup of Io when it was not covered by the slit (NIRSPEC-6 blocking filter). Panel (c) shows a fraction of a spectrum of Io in eclipse, taken with the NIRSPEC-6a blocking filter. Wavelength increases from the top to the bottom, and distance along the slit is along the x axis. Since two spectra were subtracted from each other, a positive and negative spectral trace are shown. The horizontal stripes are residual lines in our own atmosphere; these are removed from the final spectrum (Fig. 2) as described in the text. Superposed is a scan through the traces to show the relative intensities. The bright knots on the positive and negative trails, roughly aligned with the scan, are caused by the SO emission band.

is obtained for 825 ± 25 K. Although this fits the data shortwards of 2 μm quite well, it is too flat at longer wavelengths. A better fit to the slightly curved spectrum is obtained with a region consisting of two temperatures. The best two-temperature fit is obtained for a region at 960 ± 12 K, together with a 25 times larger area at 640 ± 5 K. We will show in a future paper that the addition of the mid-IR data obtained simultaneously at Keck I calls for the addition of lower temperature regions, covering larger surface areas.

To establish an absolute calibration scale, we used SCAM images of the photometric star SJ9182 and of Io through the NIRCSPEC-6 (1.57–2.35 μm) blocking filter, when the objects were not on the spectrometer slit. This resulted in a total photon flux of 17 ± 3 photons s^{-1} cm^{-2} μm^{-1} for Io. We used this number to determine the absolute scale of our two-temperature blackbody fit and derived areas (as projected on the sky) of $\sim$2.0 km^2 for the 960 K hot spot and $\sim$50 km^2 for the 640 K spot. The dashed line in Fig. 2b shows this blackbody curve superposed on the observed NIRSPEC spectrum. This curve, when convolved with the filter response, gives a flux of 17 ± 3 photons s^{-1} cm^{-2} μm^{-1}.

Emission band identification. It is clear from Fig. 2 that we detected an emission band at 1.7 μm. We identify this band with the 0–0 vibrational band of the $a^1\Delta \rightarrow X^3\Sigma^-$ electronic transition of the SO radical. The $a^1\Delta$ state is a metastable excited state, with $X^3\Sigma^-$ as the ground state. A total of 225 rovibronic lines are known across the band, distributed over nine rotational branches (Setzer *et al.* 1999). To show the similarity of our spectrum to the laboratory data, we convolved the laboratory data with a Gaussian with a full width at half maximum of 8.5 Å ($R = 2000$ at 1.7 μm) and show the result (scaled to the observed peak intensity) as a red line overplotted in Fig. 2c. We caution the reader that the laboratory data are not corrected for variations in the sensitivity of the germanium detector as a function of wavelength. The detector has maximum sensitivity near 1.54 μm, and sensitivity drops to zero near 1.75 μm. The precise detector response as a function of wavelength is not known; the intensities may drop linearly by a factor of 2–4 from 1.68 to 1.74 μm (E. Fink, private communication). However, given the good agreement of the laboratory spectrum with our model at 322 K (see below and Fig. 2d), we believe that the variations in detector sensitivity with wavelength may be overstated. Based upon a similarity of the laboratory data and our observed spectrum, we identify the emission feature with the SO $a^1\Delta \rightarrow X^3\Sigma^-$ rovibronic transition. Despite the similarity, though, several differences are apparent: Our observed band shows a clear shoulder at the right-hand side, from 1.71 to 1.72 μm. On the left, at $\sim$1.69 μm, is an unidentified peak. Although the wavelength of this peak corresponds to the ^{S}R branch of the SO band, this branch is very weak in the laboratory data.

In Fig. 2d we superpose a simulated spectrum on the data. We calculated the emission intensity of each rovibronic level using the rotational line-strength factors for $a^1\Delta \rightarrow X^3\Sigma^-$ as given by Bellary and Balasubramanian (1987) for O_2 (with $\sigma = \rho = 0$) and the wavenumbers for SO as measured by Setzer *et al.* (1999). Since the laboratory data were taken at a temperature of 322 K, there are no line positions for $J > 36$. Such lines are only important at high temperatures. We calculated these positions by refitting the laboratory line positions of Setzer *et al.* (1999) and using these new spectroscopic constants to predict line positions up to $J = 65$ in our model. Results for temperatures of 322, 1000, and 1500 K are superposed on the data. The shape of the main emission band suggests a rotational temperature of the SO molecules in the $a^1\Delta$ state of $\sim$1000 K. The mismatch between data and model spectra at 1.69 μm remains. Although we suspect this emission to be also caused by SO, we have not been able to model it.

Total photon flux. By integrating over the entire observed emission band we find a total photon flux $F_{obs} = 0.048 \pm 0.008$ photons s^{-1} cm^{-2}, which we can convert into a surface brightness, $I = F_{obs}/\Omega$, if we know the solid angle, Ω, of the SO band emission. If the emission is spatially unresolved, it is diluted by the "telescope beam." Since we used a slit width of $0.76''$, and averaged over Io (diameter $\sim 1.2''$), the solid angle of the telescope beam $\Omega_1 \approx 2 \times 10^{-11}$ sr. Alternatively, the SO emission could be concentrated in just the Loki plume, which has a width of $\sim$400–500 km (Strom and Schneider 1982), and thus $\Omega_2 \approx 4 \times 10^{-13}$ sr. The smallest solid angle one could imagine would be equal to the conduit where the material is actually ejected. Assuming the photons are released isotropically by the SO radicals, the total number of photons is $N_{ph} = 4\pi I$. If the emission comes from the Loki plume (Ω_2), then $N_{ph} = 1.5 \times 10^{12}$ photons s^{-1} cm^{-2}. Multiplying N_{ph} by the emitting area (i.e., the Loki plume of 1.5×10^{15} cm^2) results in a total photon flux of 2.3×10^{27} photons s^{-1} (note that this is independent of the surface area). Based upon an ab initio calculation, Klotz *et al.* (1984) show that the Einstein A coefficient for the entire emission band is of the order of 2.2 s^{-1}, which implies (see numbers in Discussion Section) that the collisional deexcitation rate (assumed to be $\sim 5 \times 10^{-18}$ cm^3 s^{-1}, in analogy with $O_2(a^1\Delta) + SO_2$; Boodaghians *et al.* 1983) can be ignored compared to spontaneous emission. At a rotational temperature of 1000 K our calculated band profiles show that the effective band strength is $\sim$20% larger than at 322 K.

Discussion. Our observations were conducted while Io was in eclipse. During daylight, Io has a collisionally thick, but optically thin (few nanobar surface pressure), atmosphere which is primarily composed of SO_2 (Lellouch *et al.* 1990). As mentioned in the introduction, the global SO_2 atmosphere is produced partially from sublimation of SO_2 frost on the surface and is dominated by volcanic sources (e.g., Lellouch 1996). As soon as the satellite enters an eclipse, the atmospheric and surface temperatures drop, and SO_2 condenses out on a time scale $t \sim H/c_s \sim 70$ s, where the scale height $H \approx 10$ km and sound speed $c_s \approx 1.5 \times 10^4$ cm s^{-1}. The atmosphere thus collapses within a few minutes after entering the eclipse. Although SO is much more volatile than SO_2, it will still be rapidly removed from the atmosphere because SO is highly reactive with itself on the surface (Lellouch *et al.* 1996). Since we detected SO emission from Io while in eclipse, it must somehow be continuously replenished.

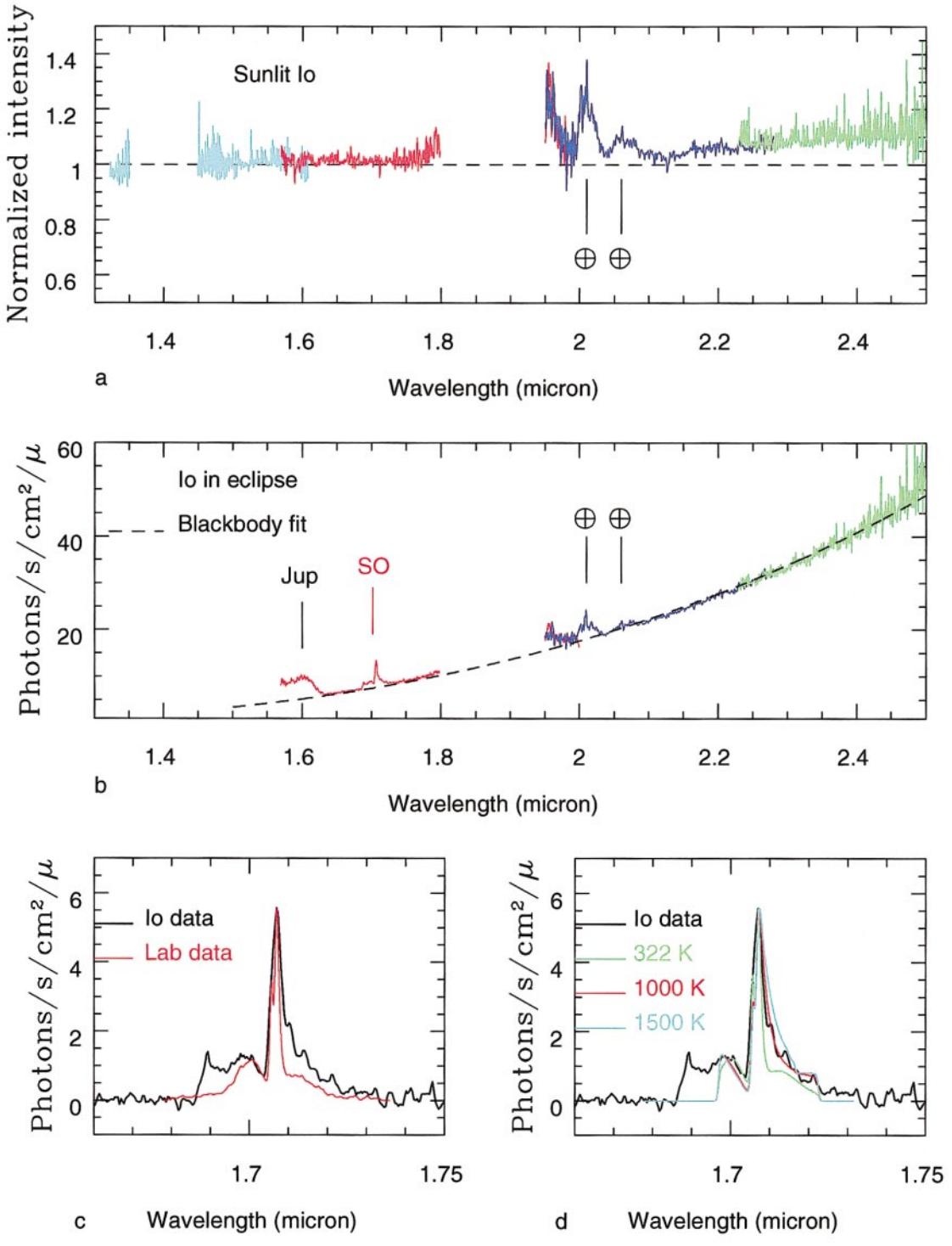

FIG. 2. Spectra of Io. (a) Spectrum of the sunlit side of the satellite, in normalized units (1 unit corresponds approximately to $\lesssim$(a few) $\times 10^4$ photons s^{-1} cm^{-2} μm^{-1}). This spectrum is composed of four different settings, indicated by the different colors (Table I). Apparent emission features caused by absorption in Earth's atmosphere are indicated by $\oplus$. (b) Spectrum of Io in eclipse. This spectrum is composed of three different settings, as indicated by the red, blue, and green colors. In addition to terrestrial atmospheric features, the SO emission band on Io and the influence of Jupiter's scattered light are indicated. (c) The SO emission band, after subtraction of the background blackbody emission. Superposed are the laboratory data (in red) from Setzer *et al*. (1999), convolved to the spectral resolution of the data. The lab spectrum has been scaled to the peak intensity of the Io data. (d) Superposed on the Io data are three models, as described in the text. We used rotational temperatures of 322 K (green; comparable to the lab data in panel (c)), 1000 K (red), and 1500 K (light-blue).

The highly forbidden nature of the electronic $a^1\Delta \rightarrow X^3\Sigma^-$ transition eliminates any possible role of solar photoexcitation. In addition to simple thermochemical equilibrium of the SO $a^1\Delta$ level with the ground $X^3\Sigma^-$ state, the only possible "excitation" process is electron impact, where electrons excite SO directly, or dissociate SO_2 while leaving SO in the $a^1\Delta$ metastable excited state. We show in the following that neither of these processes, nor ionospheric recombination of SO_2^+, are viable processes. The only plausible explanation for the observed SO emissions is direct ejection of excited SO from the volcanic vent. We discuss this scenario first.

It is possible that in the explosive, high-temperature eruption of SO_2 gas from Loki there are sufficient SO molecules in thermochemical equilibrium with SO_2, with a nonnegligible fraction in the excited $a^1\Delta$ state, which radiate upon exiting the volcanic vent. Based on the Kieffer (1982) models of Io volcanism, Strobel and Wolven (2001) calculated fluxes of SO_2 molecules for various reservoir boundary conditions. With Kieffer's preferred reservoir pressure of 40 bar and temperatures in the 400–1400 K range, Strobel and Wolven found fluxes of $\sim 10^{31}$ molecules s^{-1}. Based upon observations (Lellouch *et al.* 1996, McGrath *et al.* 2000) and models (Zolotov and Fegley 1998) ~10% of these molecules are SO. Assuming that the SO electronic states are in thermodynamic equilibrium, we can calculate the quenching temperature (i.e., the temperature at which the states were "equilibrated") from the observed emission rate ($\sim 2.3 \times 10^{27}$ excited SO molecules s^{-1}, or ~0.02% of Strobel and Wolven's venting rate) using Boltzmann's equation, where the energy separation between the $a^1\Delta$ and $X^3\Sigma^-$ states is $\Delta E = 0.73$ eV. This quenching temperature appears to be about 1500 K. For Loki, one might expect lower temperatures, but shock-wave heating along the conduit or crater walls or by the Mach disk shock in the plume could augment these lower temperatures to the required 1500 K. The high rotational temperature (1000 K) as measured from the width of the emission band also hints at high gas temperatures. As the gas leaves the crater region and adiabatically expands and cools in the plume region, the various electronic, rotational, and vibrational energy levels relax to the lower temperatures. Because interconversion of rotational and translational energy only requires tens of collisions in comparison to $\sim 10^8$ collisions for interconversion of electronic ($a^1\Delta$) and translational energy in the O_2 molecule (Boodaghians e*t al.* 1983), one would expect a much higher quenching temperature for the SO($a^1\Delta$) state, as indeed the data suggest, than for rotational levels.

One may wonder if it would not be possible for the SO electronic states to be in thermodynamical equilibrium at ~2000 K, the temperature expected at subnanobar pressures above volcanic vents (and the upper atmosphere in general) due to Joule heating (Strobel *et al.* 1994). Indeed, in that case a column density of only 2×10^{14} cm^{-2} SO molecules in the ground $X^3\Sigma^-$ state is sufficient to sustain the observed emission rate. However, interconversion of translation energy to electronic energy is notoriously improbable for collisions with stable molecules and in Io's tenuous atmosphere it is difficult to compete with the fast radiative decay rate of 2.2 s^{-1} (Klotz *et al.* 1984) to enforce an equilibrium population of electronic states. So this scenario is not very appealing.

We now briefly summarize why electron impact and ionospheric recombination processes as mentioned above fail. It would indeed be tempting to assume electron impact excitation of the ground state of SO as the source of the emission band:

$$e^- + \mathrm{SO}(X^3\Sigma^-) \rightarrow \mathrm{SO}(a^1\Delta) + e^-. \quad (1)$$

In the absence of laboratory measurements for SO, we use the equivalent cross section for O_2 (Shyn and Sweeney 1993): $e^- + O_2(X^3\Sigma^-) \rightarrow O_2(a^1\Delta) + e^-$. Typical electron densities in the Io plasma torus are ~2000–3000 cm^{-3} at temperatures of ~5–6 eV (Sittler and Strobel 1987). When integrating the equivalent cross section for O_2 over a Maxwellian distribution of electrons at a temperature of 5 eV, we obtain a collisional excitation rate of 9×10^{-10} cm^3 s^{-1} per electron, or an overall excitation rate of $\sim 3 \times 10^{-6}$ s^{-1}. Thus a column density of 5×10^{17} SO cm^{-2} is needed to explain our observed flux. However, 5-eV electrons can penetrate through, at most, a column density of 10^{15} molecules cm^{-2} before depleting all of their energy. Therefore, this scenario is not viable.

Electron impact dissociation of SO_2 into excited SO is another possibility:

$$e^- + \mathrm{SO}_2 \rightarrow \mathrm{SO}(a^1\Delta) + \mathrm{O}(^1D, ^3P) + e^-. \quad (2)$$

However, no measured cross sections are available for these channels. Based upon measurements of the total electron impact dissociation rate of SO_2 (Vuskovic and Trajmar 1982), we estimate an upper limit for the dissociation rate in (2) of 7×10^{-9} cm^3 s^{-1} per electron at 5 eV and a maximum rate of $\sim 6 \times 10^{-8}$ cm^3 s^{-1} at 55 eV, which imply overall rates of 2×10^{-5} and 2×10^{-4} s^{-1}, respectively, for torus electrons, and corresponding SO_2 column densities of 7×10^{16} and 8×10^{15} cm^{-2}. These column densities are much larger than the 10^{15} cm^{-2} the electrons can penetrate.

Io's ionosphere is created primarily via collisions with torus electrons (Saur *et al.* 1999). Typical electron densities are $\gtrsim 10^5$ cm^{-3} (Hinson *et al.* 1998), but these electrons are much colder than torus electrons (0.2–1 eV?), so that the SO and SO_2 column densities need to be even higher than in the previous cases to explain the observed emissions. Ionospheric recombination of $SO_2^+ + e^-$ is another possible source of excited SO, assuming this yields preferentially SO($a^1\Delta$) + O. Using a recombination rate of 7×10^{-8} cm^3 s^{-1} at electron temperatures $T_e = 0.2$ eV, we estimate that the ionospheric number density required to yield the observed emission rate needs to be 2×10^6 cm^{-3} (and higher still at $T_e = 1$ eV). Since this is an order of magnitude higher than was observed by Hinson *et al.* (1998), the SO emission cannot be caused by ionospheric recombination of SO_2.

Conclusions. We detected the forbidden electronic $a^1\Delta \rightarrow X^3\Sigma^-$ transition of the SO radical at 1.7 μm on Io while eclipsed by Jupiter. We investigated a number of scenarios to explain the observed emission and conclude that we most likely detect the photons emitted by SO molecules which are directly ejected from the vent in the excited $a^1\Delta$ state. If we assume a SO/SO_2 abundance ratio of ~0.1, and a venting rate of $\sim 10^{31}$ molecules s^{-1} (Strobel and Wolven 2001), we find that the thermodynamic quenching temperature of the SO ($a^1\Delta$) state is ~1500 K. We used the shape of the SO emission band to derive a rotational temperature of 1000 K for the gas. Although this is a very high gas temperature, it is less than the thermodynamic quenching temperature, as expected. The constancy of the line-to-continuum ratio in the SO band over the time span (~3/4 h) of our observations suggests that the volcanic eruption must have been very stable over at least hour-long time scales. Finally, we note that there still is an, as of yet unexplained, emission peak at 1.69 μm.

If indeed we have detected SO directly escaping from the vent, this presents a new way to monitor Io's volcanic activity, where we infer the combination of a SO ejection rate (high/low) and corresponding (lower/higher) quenching temperature of the excited state. In the future, we will attempt observations of both the SO $a^1\Delta$ and $b^1\Sigma^+ \rightarrow X^3\Sigma^-$ transitions in the conventional way as well as using an adaptive optics system to retrieve information on the spatial scale (at a resolution of ~140 km) of the emitting molecules.

Acknowledgments. We greatly appreciate our correspondence with Dr. Ewald Fink, who sent us the SO $a^1\Delta \rightarrow X^3\Sigma^-$ laboratory data for comparison with our spectrum. We thank Dr. Ewine van Dishoeck for bringing the authors together. Partial support for this work (to P.B.) was provided by the Natural Sciences and Engineering Council of Canada and the NASA Laboratory Astrophysics program. D.F.S. acknowledges support by NASA Grant NAG-5-4168. The data presented were obtained at the W. M. Keck Observatory, which is operated as a scientific partnership among the California Institute of Technology, the University of California, and the National Aeronautics and Space Administration. The Observatory was made possible by the generous financial support of the W. M. Keck Foundation. The authors extend special thanks to those of Hawaiian ancestry on whose sacred mountain we are privileged to be guests. Without their generous hospitality, none of the observations presented would have been possible.

REFERENCES

Ballester, G. E., M. A. McGrath, D. F. Strobel, X. Zhu, P. D. Feldman, and H. W. Moos 1994. Detection of the SO_2 atmosphere on Io with the Hubble Space Telescope. *Icarus* **111**, 2–17.

Bellary, V. P., and T. K. Balasubramanian 1987. On the rotational intensity distribution in the $a^1\Delta_g \rightarrow X^3\Sigma_g^-$ magnetic dipole transition of oxygen molecule. *J. Mol. Spectrosc.* **126**, 436–442.

Boodaghians, R. B., P. M. Borrell, and P. Borrell 1983, Room-temperature rate constants for the gas-phase quenching of metastable molecular oxygen, $O_2(a^1\Delta_g)$ and $O_2(b^1\Sigma_g^+)$, by CO_2, N_2O, NO, NH_3, HCl, and SO_2. *Chem. Phys. Lett.* **97**, 193–197.

Colina, L., R. C. Bohlin, and F. Castelli 1996. The 0.12–2.5 micron absolute flux distribution of the Sun for comparison with solar analog star. *Astron. J.* **112**, 307–315.

Douté, S., B. Schmitt, R. Lopes-Gautier, R. Carlson, L. Soderblom, J. Shirley, and the Galileo NIMS Team 2001. Mapping SO_2 frost on Io by the modeling of NIMS hyperspectral images. *Icarus* **149**, 107–132.

Hinson, D. P., A. J. Kliose, F. M. Flasar, J. D. Twicken, P. J. Schinder, and R. G. Herrera 1998. Galileo radio occultation measurements of Io's ionosphere and plasma wake. *J. Geophys. Res.* **103**, 29,343–29,357.

Howell, R. R., and 13 colleagues 2001. Ground based observations of volcanism on Io in 1999 and early 2000. *J. Geophys. Res*, in press.

Kieffer, S. W. 1982, Dynamics and thermodynamics of volcanic eruptions: Implications for the plumes of Io. In *Satellites of Jupiter* (D. Morrison, Ed.), pp. 647–723. Univ. of Arizona Press, Tucson.

Klotz, R., C. M. Marian, S. D. Peyerimhoff, B. A. Hess, and R. J. Buenker 1984. Calculation of spin-forbidden radiative transitions using correlated wavefunctions: Lifetimes of $b^1\Sigma^+$, $a^1\Delta$ states in O_2, S_2, and SO. *Chem. Phys.* **89**, 223–236.

Lellouch, E. 1996. Urey Prize lecture. Io's atmosphere: Not yet understood. *Icarus* **124**, 1–21.

Lellouch, E., M. J. S. Belton, I. de Pater, S. Gulkis, and T. Encrenaz 1990. Io's atmosphere from microwave detection of SO_2. *Nature*, **346**, 639–641.

Lellouch, E., M. Belton, I. de Pater, G. Paubert, S. Gulkis, and Th. Encrenaz 1992. The structure, stability, and global distribution of Io's atmosphere. *Icarus* **98**, 271–295.

Lellouch, E., D. F. Strobel, M. J. S. Belton, M. E. Summers, G. Paubert, and R. Moreno 1996. Detection of sulfur monoxide in Io's atmosphere. *Astrophys. J.* **459**, L107–110.

Lopes, R., L. Kamp, S. Douté, and the Galileo NIMS Team 2001. Io in the near infrared: NISM results from the Galileo fly-bys in 1999 and 2000. *J. Geophys. Res.*, submitted.

McLean, I., J. R. Graham, E. E. Becklin, D. F. Figer, J. E. Larkin, N. A. Levenson, and H. I. Teplitz 2000. Performance and results with the NIRSPEC echelle spectrograph on the Keck II telescope. *Proc. SPIE* **4008**, 1048–1055.

McGrath, M. A., M. J. S. Belton, J. R. Spencer, and P. Sartoretti 2000. Spatially resolved spectroscopy of Io's Pele plume and SO_2 atmosphere. *Icarus* **146**, 476–493.

Pearl, J. R., R. A. Hanel, V. Kunde, W. Maguire, W. Fox, S. Gupta, C. Ponnamperuma, and F. Raulin 1979. Identification of gaseous SO_2 and new upper limits for other gases on Io. *Nature* **280**, 757–758.

Persson, S. E., D. C. Murphy, W. Krzeminski, M. Roth, and M. J. Rieke 1998. A new system of faint near-infrared standard stars. *Astron. J.* **116**, 2475–2488.

Saur, J., F. M. Neubauer, D. F. Strobel, and M. E. Summers 1999. 3D plasma simulations of Io's interaction with the Io plasma torus: Asymmetric plasma flow. *J. Geophys. Res.* **104**, 25,105–25, 126.

Setzer, K. D., E. H. Fink, and D. A. Ramay 1999. High-resolution Fourier-transform study of the $b^1\Sigma^+ \rightarrow X^3\Sigma^-$ and $a^1\Delta \rightarrow X^3\Sigma^-$ transitions of SO. *J. Mol. Spectrosc.* **198**, 163–174.

Shyn, T. W., and C. J. Sweeney 1993. Differential electronic-excitation cross sections of molecular oxygen by electron impact: The $a^1\Delta_g$ and $b^1\Sigma_g$ states. *Phys. Rev. A* **47**, 1006–1008.

Sittler, E. C., Jr., and D. F. Strobel 1987. Io plasma torus electrons: Voyager 1. *J. Geophys. Res.* **92**, 5741–5762.

Strobel, D. F., X. Zhu, and M. E. Summers 1994. On the vertical thermal structure of Io's atmosphere. *Icarus* **111**, 18–30.

Strobel, D. F., and B. C. Wolven 2001. The atmosphere of Io: Abundances and sources of sulfur dioxide and atomic hydrogen. *Astrophys. Space Sci.* **277**, 1–17.

Strom, R. G., and N. M. Schneider 1982. Volcanic eruption plumes of Io. In *Satellites of Jupiter* (D. Morrison, Ed.), pp. 598–633. Univ. of Arizona Press, Tucson.

Vuskovic, L., and S. Trajmar 1982. Electron impact excitation of SO_2: Differential, integral, and momentum transfer cross sections. *J. Chem. Phys.* **77**, 5436–5440.

Zolotov, M. Y., and B. Fegley Jr. 1998. Volcanic production of sulfur monoxide (SO) on Io. *Icarus* **132**, 431–434.